Dysfunctional cardiac mitochondrial bioenergetic, lipidomic, and signaling in a murine model of Barth syndrome[S]

Michael A. Kiebish,[1,*] Kui Yang,[*] Xinping Liu,[*] David J. Mancuso,[*] Shaoping Guan,[*] Zhongdan Zhao,[*] Harold F. Sims,[*] Rebekah Cerqua,[*] W. Todd Cade,[†] Xianlin Han,[2,*] and Richard W. Gross[3,*,§,]**

Division of Bioorganic Chemistry and Molecular Pharmacology, Departments of Medicine,[*] Physical Therapy,[†] and Developmental Biology,[§] Washington University School of Medicine, St. Louis, MO 63110; and Department of Chemistry,[**] Washington University, St. Louis, MO 63130

Abstract **Barth syndrome is a complex metabolic disorder caused by mutations in the mitochondrial transacylase tafazzin. Recently, an inducible tafazzin shRNA knockdown mouse model was generated to deconvolute the complex bioenergetic phenotype of this disease. To investigate the underlying cause of hemodynamic dysfunction in Barth syndrome, we interrogated the cardiac structural and signaling lipidome of this mouse model as well as its myocardial bioenergetic phenotype. A decrease in the distribution of cardiolipin molecular species and robust increases in monolysocardiolipin and dilysocardiolipin were demonstrated. Additionally, the contents of choline and ethanolamine glycerophospholipid molecular species containing precursors for lipid signaling at the *sn*-2 position were altered. Lipidomic analyses revealed specific dysregulation of HETEs and prostanoids, as well as oxidized linoleic and docosahexaenoic metabolites. Bioenergetic interrogation uncovered differential substrate utilization as well as decreases in Complex III and V activities. Transgenic expression of cardiolipin synthase or iPLA$_2\gamma$ ablation in tafazzin-deficient mice did not rescue the observed phenotype. These results underscore the complex nature of alterations in cardiolipin metabolism mediated by tafazzin loss of function. Collectively, we identified specific lipidomic, bioenergetic, and signaling alterations in a murine model that parallel those of Barth syndrome thereby providing novel insights into the pathophysiology of this debilitating disease.**—Kiebish, M. A., K. Yang, X. Liu, D. J. Mancuso, S. Guan, Z. Zhao, H. F. Sims, R. Cerqua, W. T. Cade, X. Han, and R. W. Gross. **Dysfunctional cardiac mitochondrial bioenergetic, lipidomic, and signaling in a murine model of Barth syndrome.** ***J. Lipid Res.*** **2013.** 54: **1312–1325.**

Supplementary key words lipidome • cardiolipin • tafazzin • phospholipase • mitochondria • cardiolipin synthase • transgenic • electron transport chain

Barth syndrome is an X-linked complex metabolic disorder caused by mutations in the gene tafazzin (1–4). Clinical manifestations of Barth syndrome include growth delay, hypertrophic or dilated cardiomyopathy, exercise intolerance (5), chronic or cyclic neutropenia, and 3-methylglutaconic aciduria type II, as well as accumulation in monolysocardiolipin (MLCL) which has characteristically defined Barth syndrome as a mitochondrial lipid disorder (6, 7). Tafazzin is a transacylase which sculpts the mitochondrial lipidome, most notably cardiolipin, to maintain a stereoelectronic environment conducive for efficient bioenergetic function (8). However, the pleiotropic roles of tafazzin and cardiolipin (as well as its downstream sequelae) in regulating cellular signaling through modulation of metabolic efficiency, membrane dynamics, and multiple other mitochondrial functions have remained enigmatic (9). Recently, an inducible tafazzin shRNA knockdown (Taz KD) mouse model of Barth syndrome was generated to gain mechanistic insights into the multifaceted roles of tafazzin and cardiolipin, to increase our understanding of the complexity of alterations in Barth syndrome, and to develop

This work was supported, in whole or in part, by National Institutes of Health Grant 5PO1HL-57278 as well as a grant provided by the Barth Syndrome Foundation to M.A.K. R.W.G. has financial relationships with Lipospectrum and Platomics. X.H. has a financial relationship with Lipospectrum.

Manuscript received 7 December 2012 and in revised form 8 February 2013.

Published, JLR Papers in Press, February 12, 2013
DOI 10.1194/jlr.M034728

Abbreviations: ANT, adenine nucleotide translocase; CLS, cardiolipin synthase; CLS-TG, cardiolipin lipase transgenic; D, diacyl; DCIP, 2,6-dichloroindophenol; DLCL, dilysocardiolipin; GSEA, Gene Set Enrichment Analysis; KO, knockout; MLCL, monolysocardiolipin; P, plasmenyl; Taz KD, tafazzin shRNA knockdown.

[1] Present address of M. A. Kiebish: Berg Diagnostics, Natick, MA.
[2] Present address of X. Han: Diabetes and Obesity Research Center, Sanford-Burnham Medical Research Institute, Orlando, FL.
[3] To whom correspondence should be addressed.
e-mail: rgross@wustl.edu

[S] The online version of this article (available at http://www.jlr.org) contains supplementary data in the form of one figure.

novel therapeutic approaches for treatment of this lethal disease.

Regulation and maintenance of the mitochondrial lipidome is critical for bioenergetic efficiency, cellular signaling, and multiple other mitochondrial processes (e.g., fusion and fission) (10–13). Mitochondria are comprised of a unique double bilayer membrane structure that facilitates the compartmentalization of multiple processes to efficiently integrate mitochondrial function with cellular energy needs (11, 14, 15). A prominent lipid regulator of mitochondrial inner membrane surface charge, molecular dynamics, and membrane curvature is cardiolipin, which contains a unique tetra-acyl structure (12, 15, 16). Cardiolipin is a doubly charged mitochondrial phospholipid comprised of two phosphates, three glycerol groups, and four acyl chains (17–19). Regulation of the content and molecular species composition of cardiolipin is critical for electron transport chain efficiency, adenine nucleotide translocase activities, mitochondrial protein import, and uncoupling, as well as TCA cycle flux (20, 21). The molecular species composition of cardiolipin is dynamically regulated by integrated cellular control of cardiolipin de novo synthesis, phospholipase-mediated deacylation, and membrane remodeling by the subsequent actions of either transacylase or acyltransferase activities that are coordinately regulated to lead to a mature cardiolipin molecular species distribution (22). Additionally, because the remodeling of cardiolipin through transacylation harvests acyl chains from choline and ethanolamine glycerophospholipids, the dynamic balance of cardiolipin remodeling by transacylation versus acyltransferase activity is critical for the maintenance of mitochondrial membrane architecture, surface charge, and molecular dynamics. Thus, the precisely regulated balance of cardiolipin synthesis, remodeling, and degradation exerts tight regulatory control of mitochondrial membrane structure and function.

Herein, we examined the bioenergetic, lipidomic, and signaling mechanisms that were altered in a tafazzin loss-of-function mouse model (23–25) that was predicted to recapitulate the pathology of Barth syndrome in an animal model thereby facilitating a greater understanding of the multiple processes contributing to hemodynamic dysfunction in Barth syndrome. Through utilization of integrated molecular, chemical, and lipidomic approaches in conjunction with high-resolution respirometry, multiple novel mechanistic roles of tafazzin in regulating cardiolipin and lysocardiolipin homeostasis and myocardial signaling have been identified and their resultant effects on mitochondrial electron transport chain function, bioenergetics, and cardiac transcriptomic networks delineated. Additionally, we employed double crosses of genetic models of key enzymes involved in the cardiolipin remodeling process, namely cardiac myocyte-specific transgenic expression of cardiolipin synthase as well as the ablation of $iPLA_2\gamma$ in the Taz KD mouse model of Barth syndrome to investigate potential therapeutic strategies to attenuate maladaptive cardiolipin remodeling. Thus, through the utilization of complementary transgenic approaches, penetrating mechanistic insights into the role of tafazzin in regulating mitochondrial lipidomics, signaling, and bioenergetic function have been defined, thereby identifying the complexity of alterations resulting from tafazzin loss of function and the multiple pathologies manifest in Barth syndrome patients.

MATERIALS AND METHODS

Materials

Synthetic phospholipids used as internal standards in mass spectrometric analyses were purchased from Avanti Polar Lipids (Alabaster, AL). Solvents for sample preparation and mass spectrometric analysis were purchased from Burdick and Jackson (Muskegon, MI) as well as Sigma Aldrich (St. Louis, MO).

Induction of the doxycycline inducible Taz KD mouse model of Barth syndrome

Developmental doxycycline induction of the Taz KD mouse model was performed in utero and maintained postnatally as previously described in detail (24). A syngeneic transgenic colony was generated by breeding several generations onto a C57BL/6J mouse background, which were used for all studies. Briefly, dams were fed a 625 mg/kg doxycycline diet (Harlan Teklan) for 5 days prior to mating. Upon initiation of mating with a shRNA tafazzin-positive heterozygote male, the diet was removed for 3 days until a confirmation of insemination was obtained at which time the male was removed from the cage and the doxycycline diet was returned to the breeding cage and maintained until the pups were weaned. The genotype of the mice was confirmed by PCR as previously described (24) and male wild-type littermates and Taz KD mice were maintained on the doxycyline diet until two months of age at which time lipidomics and biochemical experiments were performed for developmental characterization. Additional experiments were performed utilizing double genetic crossed mice [Taz KD×cardiolipin synthase transgenic (CLS-TG) and Taz KD×$iPLA_2\gamma$ knockout (KO)]. In these experiments, male mice were raised until 2 months of age without doxycycline induction and at 2 months of age the mice were induced with doxycyline until 4 months of age at which time the mice were sacrificed and experiments were performed. All wild-type mice were also maintained on a 625 mg/kg doxycycline diet as control. All animal procedures were performed in accordance with the Guide for the Care and Use of Laboratory Animals and were approved by the Animal Studies Committee at Washington University School of Medicine.

Multidimensional mass spectrometry-based shotgun lipidomic analysis of the cardiac lipidome

Briefly, myocardial tissue was removed, washed with 10× diluted PBS and freeze clamped in liquid nitrogen for lipidomic analysis. Lipidomic analyses were performed as previously described, using a modified Bligh and Dyer extraction protocol (26–28). Individual lipid extracts were reconstituted with 1:1 (v/v) $CHCl_3/CH_3OH$, flushed with nitrogen, and stored at −20°C prior to electrospray ionization-MS using a TSQ Quantum Ultra Plus triple-quadrupole mass spectrometer (Thermo Fisher Scientific, San Jose, CA) equipped with an automated nanospray apparatus (Advion Biosciences Ltd., Ithaca, NY) and customized sequence subroutine operated under Xcalibur software. Enhanced MDMS-SL analysis of cardiolipins was performed with a mass resolution setting of 0.3 Thomson as described previously in detail (29).

Oxidized lipid metabolite analysis

Tissues (~100 mg) were quickly washed with cold PBS (pH 7.4) solution, blotted, snap-frozen in liquid nitrogen, and stored at −80°C until extraction. For extraction, 2 ml of ice-cold methanol/$CHCl_3$ (1:1 v/v with 1% HAc) and 2 μl of antioxidant mixture (0.2 mg/ml BHT, 0.2 mg/ml EDTA, 2 mg/ml triphenylphosphine, and 2 mg/ml indomethacin in a solution of 2:1:1 methanol/ethanol/water) were added to the tissue samples. Internal standards (250 pg each of TXB2-d4, PGE2-d4, LTB4-d4, 12-HETE-d8, 13-HODE-d4, and 9,10-DiHOME-d4 in 5 ul acetonitrile) were also added at this step. The samples were immediately homogenized and subsequently vortexed several times during a 15 min incubation on ice. Next, 1 ml of ice-cold water was added to the sample which was briefly vortexed and centrifuged at 1,500 *g* for 15 min. The $CHCl_3$ layer was transferred to a new tube and the remaining methanol/water layer was reextracted with 1 ml of $CHCl_3$ and centrifuged at 1,500 *g* for 15 min. The combined $CHCl_3$ layers were dried down with N_2 and reconstituted in 1 ml of 10% methanol solution.

The reconstituted solution was immediately applied to a Strata-X solid phase extraction cartridge that had been preconditioned with 1 ml of methanol followed by 1 ml of 10% methanol. The cartridge was then washed with 2× 1 ml of 5% methanol and additional solvent was flushed out with N_2 at a pressure of 5 psi. Eicosanoids were eluted with 1 ml of methanol containing 0.1% HAc. All cartridge steps were carried out using a vacuum manifold attached to a house vacuum line. After the organic solvent was evaporated with a SpeedVac, the residues were derivatized with *N*-(4-aminomethylphenyl)pyridinium (AMPP).

The derivatization with AMPP was performed as previously described in detail (30). Briefly, 12.5 μl of ice-cold acetonitrile/*N*,*N*-dimethylformamide (4:1, v:v) was added to the residue in the sample vial. Then 12.5 μl of ice-cold 640 mM [3-(dimethylamino) propyl]ethyl carbodiimide hydrochloride in HPLC grade water was added. The vial was briefly vortexed and 25 μl of 5 mM *N*-hydroxybenzotriazole/15 mM AMPP in acetonitrile was added. The vials were vortexed briefly and placed in a 60°C water bath for 30 min.

Arachidonic acid, linoleic acid, and docosahexaenoic acid metabolites were analyzed by LC/MS/MS. The metabolites were separated on a C18 reversed phase column (Ascentis Express, 2.7 μm particles, 150 × 2 mm), which was maintained at ambient temperature, using a mobile phase gradient (A, 0.1% glacial acetic acid in water; B, 0.1% glacial acetic acid in acetonitrile) at a flow rate of 0.2 ml/min. The solvent gradient program was 0–1.0 min, 5–20% B; 1.0–7.0 min, 20–25% B; 7.0–7.1 min, 25–40% B; 7.1–20 min, 40–60% B; 20–21 min, 60–100% B; 21–24 min, 100% B; and 24–25 min, 100% B to 5% B. A 20 min column was performed followed by equilibration of the column at 5% B for the next sample run.

Metabolites were analyzed using a hybrid tandem mass spectrometer (LTQ-Orbitrap, Thermo Scientific) via selected reaction monitoring in positive ion mode with sheath, auxiliary, and sweep gas flows of 30, 5, and 1, respectively. The capillary temperature was set to 275°C and the electrospray voltage was 4.1 kV. Capillary voltage and tube lens were set to 2 and 100 V, respectively. Instrument control and data acquisition were performed using the Thermo Xcalibur V2.1 software.

Mitochondrial high-resolution respirometry

Mice used for experiments were sacrificed and the hearts were immediately removed and dissected on ice (4°C ambient temperature). Briefly, the dissected heart was placed in mitochondrial isolation buffer (MIB) (0.21 M mannitol, 70 mM sucrose, 0.1 mM potassium-EDTA, 1 mM EGTA, 10 mM Tris-HCL, 0.5% BSA, pH 7.4) and homogenized using 12–15 passes with a Teflon homogenizer using a rotation speed of 120 rpm. Next, the homogenate was centrifuged for 5 min at 850 *g*, and the supernatant was collected and centrifuged at 7,200 *g* for 10 min. The pellet was collected and resuspended in MIB without BSA. Mitochondrial protein content was determined using a BCA protein assay (Thermo Fisher Scientific, San Jose, CA). High-resolution respirometry was performed using 50 μg of mitochondrial protein per 2 ml chamber with the substrate and inhibitor addition protocol previously described (27, 31).

Enzymatic characterization of electron transport chain and functional adenine nucleotide translocase activities

Complex I. Complex I (NADH-ubiquinone oxidoreductase) activity was determined by measuring the decrease in the concentration of NADH at 340 nm and 37°C as previously described (32, 33). The assay was performed in buffer containing 50 mM potassium phosphate (pH 7.4), 2 mM KCN, 5 mM $MgCl_2$, 2.5 mg/ml BSA, 2 μM antimycin, 100 μM decylubiquinone, and 0.3 mM K_2NADH. The reaction was initiated by adding purified mitochondria (5 μg). Enzyme activity was measured for 5 min and values were recorded 30 s after the initiation of the reaction. Specific activities were determined by calculating the slope of the reaction in the linear range in the presence or absence of 1 μM rotenone (Complex I inhibitor).

Complex II. Complex II (succinate decylubiquinone 2,6-dichloroindophenol (DCIP) oxidoreductase) activity was determined by measuring the reduction of DCIP at 600 nm as previously described (33, 34). The Complex II assay was performed in buffer containing 25 mM potassium phosphate (pH 7.4), 20 mM succinate, 2 mM KCN, 50 μM DCIP, 2 μg/ml rotenone, and 2 μg/ml antimycin. Purified mitochondria (5 μg) were added prior to initiation of the reaction. The reaction was initiated by adding 56 μM decylubiquinone. Specific activities were determined by calculating the slope of the reaction in the linear range in the presence or absence of 0.5 mM thenoyltrifluoroacetone (Complex II inhibitor).

Complex III. Complex III (ubiquinol-cytochrome c reductase) activity was determined by measuring the reduction of cytochrome c at 550 nm and 30°C. The Complex III assay was performed in buffer containing [25 mM potassium phosphate (pH 7.4), 1 mM EDTA, 1 mM KCN, 0.6 mM dodecyl maltoside, and 32 μM oxidized cytochome c] using purified mitochondria (1 μg). The reaction was initiated by adding 35 μM decylubiquinol. The reaction was measured following the linear slope for 1 min in the presence or absence of 2 μM antimycin (Complex III inhibitor). Decylubiquinol was made by dissolving decylubiquinone (10 mg) in 2 ml acidified ethanol (pH 2) and using sodium dithionite as a reducing agent. Decylubiquinol was further purified with cyclohexane (32, 33, 35).

Complex IV. Complex IV (cytochrome c oxidase) activity was determined by measuring the oxidation of ferrocytochrome c at 550 nm and 25°C. The Complex IV assay was performed in buffer containing [10 mM Tris-HCl and 120 mM KCl (pH 7.0)] using purified mitochondria (2.5 μg). The reaction was initiated by adding 11 μM reduced ferrocytochrome c and monitoring the slope for 30 s in the presence or absence of 2.2 mM KCN (Complex IV inhibitor) (33, 36).

Complex V. Complex V (F1 ATPase) activity was determined using a coupled reaction measuring the decrease in

NADH concentration at 340 nm and 37°C as previously described (37–39). The Complex V assay was performed in buffer containing (50 mM Tris-HCl, 25 mM KCl, 5 mM $MgCl_2$, 4 mM Mg-ATP, 200 μM K_2NADH, 1.5 mM phosphoenolpyruvate, 5 units pyruvate kinase, 5 units lactate dehydrogenase, 2.5 μM rotenone, and 2 mM KCN) using purified mitochondria (10 μg). The reaction was initiated by the addition of mitochondria and the reaction was monitored for 6 min. The slope in the linear range was used to calculate the reaction rate. Oligomycin (2.5 mg/ml) (Complex V inhibitor) was added to designated cuvettes to calculate the specific Complex V activity.

Functional adenine nucleotide translocase activity

Measurement of functional adenine nucleotide translocase (ANT) activity was performed using isolated mitochondria (50 μg) with high-resolution respirometry. Briefly, isolated mitochondria were incubated with pyruvate (5 mM)/malate (5 mM), glutamate (10 mM)/malate (5 mM), palmitoyl-L-carnitine (20 μM)/malate (5 mM), or succinate (10 mM)/rotenone (1 μM) and then stimulated with ADP (1.25 mM) for state 3 respiration. Once maximal stimulated oxygen consumption was achieved, atractyloside was injected at sequential concentrations between 50 pmol and 20 nmol to determine the linear inhibition of ANT under control of the various respiratory substrates as previously demonstrated (40–45).

Microarray analysis of the cardiac transcriptome

RNA was extracted from 2-month-old male WT and Taz KD mice using Trizol and the RNeasy extraction kit (Qiagen). RNA integrity was calculated and transcriptome analysis was performed using an Illumina BeadArray. Quantile analysis was utilized for postprocessing expression analysis.

Statistical analysis

Data were analyzed using a two-tailed unpaired Student's *t*-test. Differences were regarded as significant at the $^{*}P < 0.05$, $^{**/\#}P < 0.01$. All data are reported as the means ± SEM unless otherwise indicated.

RESULTS

Identification of the cardiac cardiolipin phenotype of the developmental inducible Taz KD mouse model of Barth syndrome

We used a multidisciplinary approach to investigate the biochemical and biophysical mechanisms leading to mitochondrial dysfunction resulting from tafazzin loss of function in mice. Mass spectrometric analysis of myocardial cardiolipin molecular species was performed by MDMS-SL analysis using the M + 1/2 isotopologue approach we previously developed (29). The results revealed dramatic alterations in cardiolipin content and molecular species distribution induced by tafazzin loss of function (**Fig. 1A**). Quantitative analysis of cardiolipin molecular species revealed a dramatic decrease in linoleic (18:2)-enriched molecular species, most notably tetra-18:2 (18:2-18:2-18:2-18:2), which is the major molecular species of cardiolipin in myocardium (Fig. 1B). Importantly, the decrease in tetra-18:2 molecular species is a hallmark characteristic of Barth syndrome (46). Selective cardiolipin molecular species containing dihomo-γ-linolenic acid (20:3) or docosahexaenoic acid (22:6) were also decreased including 18:2-18:2-18:2-20:3 and 18:2-18:2-18:2-22:6 molecular species, respectively. Additionally, immature cardiolipin species containing 16:0 and 16:1 fatty acyl chains accumulated after tafazzin knockdown including 18:2-18:1-18:1-16:0 and 18:2-18:1-18:1-16:1/18:2-18:2-18:1-16:0 molecular phosphatidylglycerol species. Quantitative analysis of lysocardiolipin revealed the accumulation of monolysocardiolipin (MLCL) molecular species in the inducible Taz KD mouse model, which were most abundantly represented by molecular species containing 18:1 and 16:0 acyl chains present in the biosynthetic precursor of CL, including 18:2-18:2-18:1, 18:2-18:1-18:1, 18:1-18:1-16:0, and 18:2-18:1-16:0 (Fig. 1C). Unexpectedly, through the power inherent in untargeted mass spectrometric approaches, shotgun lipidomic analysis revealed the accumulation of dilysocardiolipin (DLCL) molecular species, which were predominately comprised of 18:2-18:1 DLCL and 18:1-18:1 DLCL in the Taz KD mouse model. All molecular species of MLCL and DLCL were confirmed by accurate mass, MDMS-SL, and product ion analysis. Thus, the discovery of DLCL as well as the identification of key metabolic intermediate molecular species in MLCL and DLCL demonstrates the critical role of tafazzin in the addition of acyl chains to MLCL to form mature CL molecular species.

Tafazzin deficiency results in altered choline and ethanolamine glycerophospholipid molecular species

Cardiolipin molecular species remodeling involves the coordinated regulation of various phospholipase, acyltransferase, and transacylase activities. Mutants in tafazzin have previously been associated with defective transacylation of specific acyl chains from choline and ethanolamine glycerophospholipid molecular species (3, 8). In the present study, loss of tafazzin enzymatic activity in the Barth syndrome mouse model results in the accumulation of specific choline diacyl (D) glycerophospholipid molecular species containing linoleic acid in the *sn*-2 position, specifically D16:0-18:2 and D18:0-18:2 (**Fig. 2A**). Due to the increased linoleic acid content in choline glycerophospholipid molecular species, the utilization of linoleic acid to synthesize arachidonic acid by acyl chain elongation is also altered as evidenced by an increased content of 20:3- (an intermediate in the synthesis of 20:4 from 18:2) and 20:4-containing molecular species (e.g., D18:0-20:3 and D18:0-20:4). Furthermore, molecular species containing docosahexaenoic acid at their *sn*-2 positions are decreased including D16:0-22:6 and D18:2-22:6, thus demonstrating an imbalance in the architectural restructuring of choline glycerophospholipid molecular species. The increased presence of ω-6 polyunsaturated fatty acids (i.e., linoleic acid and arachidonic acid) may partially account for the deficiency of docosahexaenoic acid because the biosynthesis of both ω-6 and ω-3 polyunsaturated fatty acids compete for the same enzyme systems. Interestingly, analysis of ethanolamine glycerophospholipid molecular species also displayed an overall increase in molecular species containing

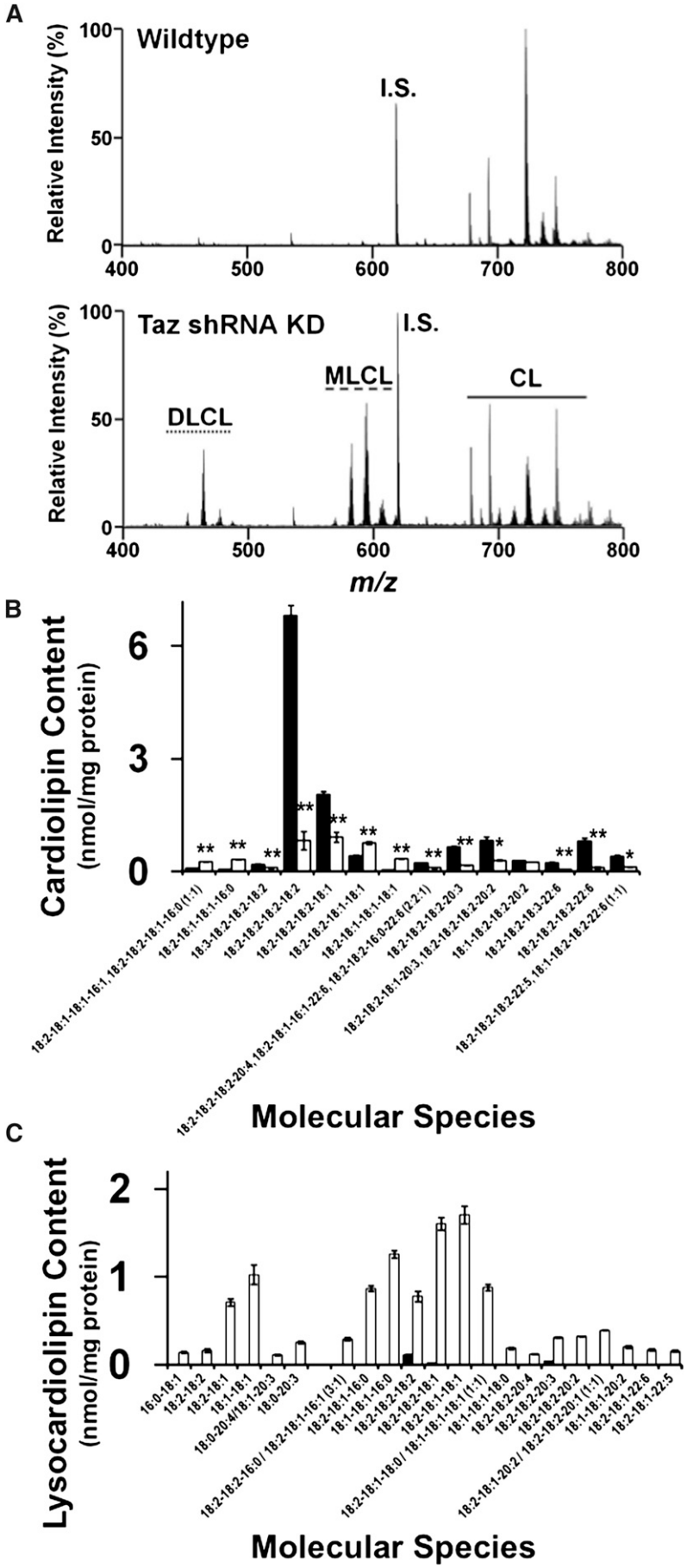

Fig. 1. Analysis of cardiolipin and lysocardiolipin in the myocardium of 2-month-old wild-type and Taz KD mice induced in utero. A: Spectral analysis of the 0.5 isotopologue of the doubly charged cardiolipin molecular species revealed a dramatic decrease in remodeled cardiolipin molecular species, especially tetra-18:2 cardiolipin (*m/z* 723.95) in Taz KD mice compared with wild-type littermates. B: Quantification of cardiolipin molecular species using the tetra-14:0 internal standard demonstrated a significant decrease in 18:2-enriched molecular species and to a much lesser extent 22:6-containing species in the Taz KD mice compared with wild-type littermates. Molecular species below 0.2 nmol/mg protein were omitted from the figure for visual clarity. C: Analysis of lysocardiolipins revealed an increase in both dilysocardiolipin and monolysocardiolipin molecular species. Molecular species below 0.1 nmol/mg protein were omitted from the figure for visual clarity. Values represent the mean quantitative value of molecular species ± S.E. (N = 3 hearts per group; black bars, wild-type littermates; white bars, Taz KD mice). $^{*}P < 0.05$ level, $^{**}P < 0.01$ level.

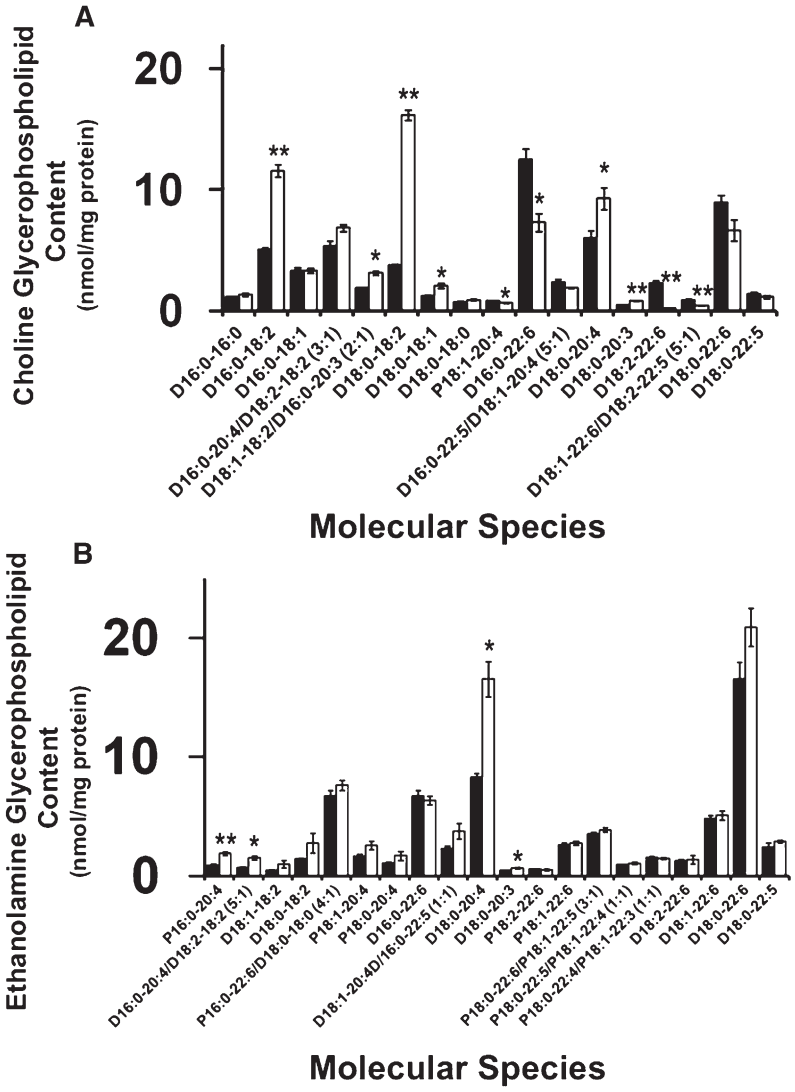

Fig. 2. Quantitation of myocardial choline and ethanolamine glycerophospholipid molecular species in the Taz KD mouse model. A: Analysis of choline glycerophospholipid molecular species revealed a selective increase in 18:2- and a decrease in 22:6-enriched molecular species. B: Analysis of ethanolamine glycerophospholipids revealed an increase in specific 20:4-containing species. Values represent the mean quantitative value of molecular species ± S.E. (N = 3 hearts per group; black bars, wild-type littermates; white bars, Taz KD mice). Values lower than 0.5 nmol/mg protein were not presented for figure clarity. $*P < 0.05$ level, $**P < 0.01$ level.

arachidonic acid at their *sn*-2 positions as evidenced by plasmenyl (P) P16:0-20:4, D16:0-20:4, and D18:0-20:4 (Fig. 2B), while molecular species containing docosahexaenoic acid remain largely unchanged including D16:0-22:6, D18:0-22:6, P16:0-22:6, and P18:0-22:6 molecular species. This overall imbalance in 18:2-, 20:4-, and 22:6-enriched molecular species driven by a deficiency to incorporate 18:2 fatty acyl groups into cardiolipin dramatically alters membrane biophysical properties and stereoelectronic relationships in the myocardium of the murine Barth syndrome model. These alterations will likely precipitate changes in the function of inner membrane protein complexes resulting in bioenergetic inefficiency and alterations in cellular signaling processes that utilize these polyunsaturated fatty acids as signaling molecules after their release by the action of phospholipases and their subsequent oxidation to biologically active signaling metabolites. Thus, the myocardial lipidome of the Taz KD demonstrated dramatic pathologic alterations in lipid composition, and by inference, alterations in membrane biophysical properties.

Decreased tafazzin activity results in altered myocardial generation of biologically potent oxidized signaling metabolites

Signaling metabolites generated from the oxidation of linoleic, arachidonic, and docosahexaenoic acids are potent mediators of calcium homeostasis, inflammation, and vascular regulation (47–51). Examination of Taz KD myocardium revealed the complex dysregulation of oxidized 18:2, 20:4, and 22:6 fatty acyl molecular species. Analysis of multiple eicosanoids revealed increases in 5-HETE and 11-HETE as well as a decrease in 15-HETE content in Taz KD compared with the wild-type littermate myocardium (**Fig. 3A**). Interestingly, cardioprotective EETs were unchanged in myocardium. Analysis of prostanoids revealed an increase in PGE_2, $PGF_{2\alpha}$, TXB_2, 6keto-$PGF_{1\alpha}$, and $PGF_{1\alpha}$ metabolites in the Barth syndrome mouse model that are likely to result in multiple pathologic alterations in inflammation, ion channel function, and cellular signaling cascades.

The alteration of 18:2 fatty acyl chains in glycerophospholipids in the Barth syndrome mouse model alters the production of signaling molecules emanating from linoleic

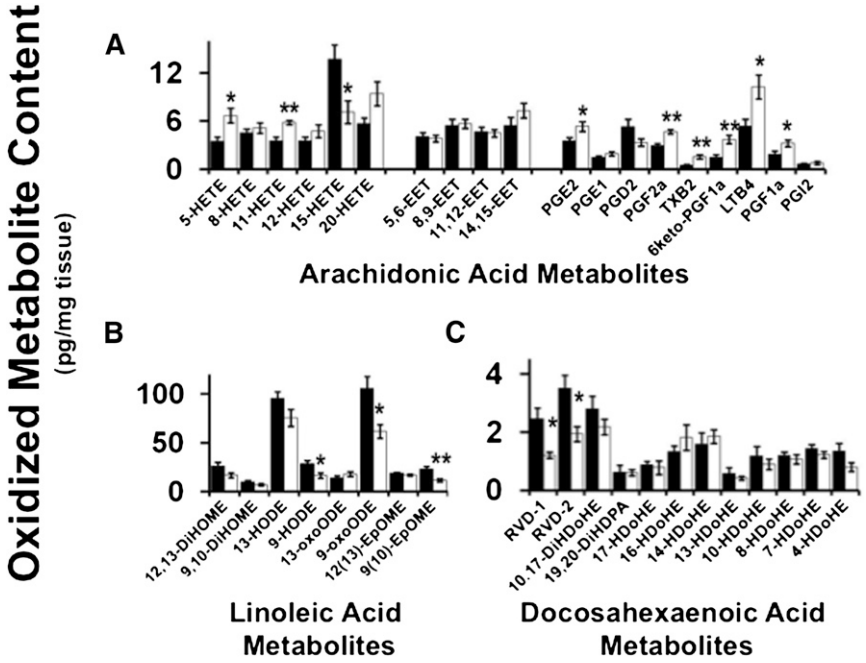

Fig. 3. Myocardial generation of oxidized fatty acid metabolites is altered in the Taz KD mouse model. A: Oxidized arachidonic acid metabolites. B: Oxidized linoleic acid metabolites. C: Oxidized docosahexaenoic acid (DHA) metabolites in wild-type and Taz KD mouse hearts. Values represent the mean (pg/mg tissue) ± S.E. (N = 6 hearts per group; black bars, wild-type littermates; white bars, Taz KD mice). *$P < 0.05$ level, **$P < 0.01$ level.

acid release by phospholipases. Analysis of the biologically potent oxidized metabolites of 18:2 fatty acid revealed decreases in 9-HODE, 9-oxoODE, and 9(10)-EpOME, but not other oxidized 18:2 derivatives, demonstrating selective metabolic channeling of the 18:2 fatty acyl chains present in phospholipids due to decreased tafazzin-mediated transacylation (Fig. 3B). Investigation of 22:6 oxidized aliphatic chain content, which would be prone to oxidation due to its high degree of unsaturation, reveals a selective decrease in the anti-inflammatory metabolites RVD1 and RVD2 in the Taz KD compared with wild-type control myocardium (Fig. 3C). In contrast, DiHDoHE, DiHDPA, and HDoHE were unchanged.

Tafazzin deficiency leads to altered myocardial substrate utilization for respiration

Alterations in the mitochondrial membrane lipidome precipitate bioenergetic inefficiency and impair adaptive alterations in substrate utilization during metabolic transitions. In the present study, redistribution of acyl chains in cardiolipin and mitochondrial glycerophospholipids in the Taz KD model resulted in a shift in mitochondrial metabolism in a substrate-specific manner. Pyruvate oxidation was unaltered in isolated mitochondria from Taz KD cardiac mitochondria compared with wild-type littermates (**Fig. 4A**). However, fatty acid oxidation utilizing palmitoyl-L-carnitine as substrate was decreased by 25% during state 3 respiration in Taz KD cardiac mitochondria compared with wild type. Moreover, this deficiency was maintained upon addition of succinate, which would combine both Complex I and Complex II electron and proton donation through the respiratory chain (Fig. 4B). Surprisingly, glutamate-stimulated oxidation was increased by 25% during state 3 respiration in cardiac mitochondria isolated from the Taz KD mice compared with wild-type littermates, which suggests a dramatic shift toward the selection of amino acids for preferential substrate oxidation (Fig. 4C). In order to test the adaptability of mitochondria to the utilization of multiple substrates entering the TCA cycle, pyruvate and glutamate were employed to determine the dynamic flux of these TCA cycle substrates used in the wild-type and the Taz KD mouse model. Utilization of pyruvate and glutamate as substrates demonstrated a 15% decrease in state 3 respiration, suggesting that the redox capacity and metabolic flexibility of the TCA cycle in isolated cardiac mitochondria from the Taz KD mice is deficient relative to wild-type littermates (Fig. 4D). Comparison of multiple substrate combinations to drive state 3 respiration by measuring substrate control ratios demonstrated that fatty acid oxidation is markedly impaired in the Taz KD mouse model, yet amino acid fermentation utilizing glutamate appears to predominate as the preferential fuel to meet energetic demands (Fig. 4E). This selective shift in substrate oxidation will lead to multiple downstream bioenergetic repercussions, because normal myocardium generally utilizes fatty acids and glucose under physiological conditions and not amino acids as a primary fuel substrate.

Inhibition of tafazzin expression precipitates alterations in Complex III, Complex V, and glutamate-stimulated adenine nucleotide translocase activities

The efficiency and enzymatic activity of the electron transport chain has been closely associated with alterations

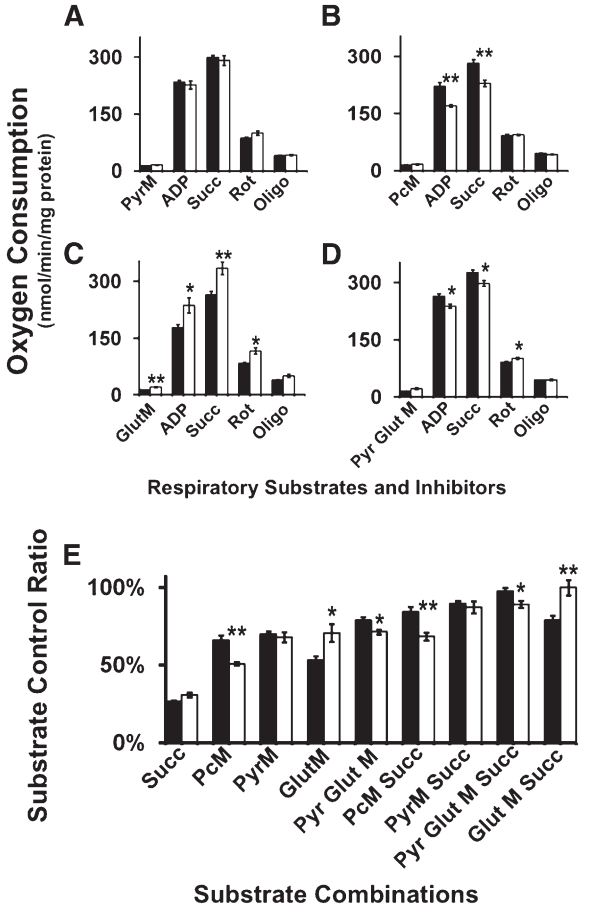

Fig. 4. Cardiac mitochondrial substrate selectivity was altered in the Taz KD mouse model. High-resolution respirometry demonstrated substrate-selective control of respiration utilizing (A) pyruvate, (B) palmitoyl-L-carnitine, (C) glutamate, and (D) pyruvate and glutamate substrates for state 3 respiration. E: Comparative analysis of substrate control ratios revealed an overall decrease in palmitoyl–L-carnitine-stimulated respiration and an increase in glutamate-stimulated respiration in Taz KD cardiac mitochondria compared with wild-type littermates. Values represent the mean oxygen consumption (nmol/min/mg mitochondrial protein) ± S.E. (N = 5 hearts per group; black bars, wild-type littermates; white bars, Taz KD mice). *$P < 0.05$ level, **$P < 0.01$ level.

in the lipid composition of mitochondrial membranes and in the content and molecular species composition of cardiolipin molecular species in particular (11, 12). Due to extensive alterations in cardiolipin molecular species composition and the accumulation of lysocardiolipin in cardiac mitochondria isolated from Taz KD mice, we measured the activities of the electron transport chain complexes in wild- type mice and the mouse model of Barth syndrome. Examination of electron transport chain activities revealed a 45% decrease in Complex III activity and a 25% decrease in Complex V activity in cardiac mitochondria isolated from Taz KD mice compared with wild-type littermates (**Fig. 5A**). These results demonstrate the essential biophysical role of alterations in mitochondrial membrane lipid composition in the Barth syndrome mouse model.

Regulation of ANT activity is partially regulated by the molecular composition of cardiolipin which has been shown to modulate ADP/ATP exchange in a substrate-specific manner to direct bioenergetic metabolite oxidation (52, 53). To investigate the differences between state 3 substrate utilization in myocardium from the murine model of Barth syndrome, we measured functional ANT activity driven by pyruvate, glutamate, palmitoyl-L-carnitine, and succinate. Analysis of functional ANT activity revealed a selective 6-fold increase in glutamate-stimulated activity in isolated cardiac mitochondria from Taz KD mice compared with wild-type littermates (Fig. 5B). This suggests that altering the mitochondrial lipidome influences the substrate selectivity of the ANT leading to downstream changes in electron transport chain flux and coupling efficiency.

Inducible Taz KD results in compensatory alterations in the myocardial transcriptome

To gain further molecular insight into the compensatory mechanisms that result from alterations in the mitochondrial lipidome and myocardial membrane remodeling, we examined the cardiac transcriptome in the Taz KD mouse model of Barth syndrome. Gene Set Enrichment Analysis (GSEA) (54, 55) revealed dramatic increases in various processes involved in amino acid synthesis, protein translation, and amino acid metabolism in addition to increases in nucleotide metabolism, GTP hydrolysis, and folate metabolism, all of which suggest dramatic compensatory metabolic alterations in response to changes in the mitochondrial lipidome and the accumulation of lysocardiolipin (**Table 1**). Pathways that were transcriptionally downregulated included branched-chain amino acid catabolism as well as valine, leucine, and isoleucine degradation. Thus, the unexpected effects of increased amino acid synthesis and intraconversion in combination with the decreased catabolism of amino acids revealed dramatic alterations in amino acid and protein metabolism in response to altered lipid remodeling in the mitochondrial membrane which collectively precipitated alterations in substrate utilization.

Removal of doxycycline from the diet for 2 months attenuates bioenergetic and lipidomic dysfunction in the inducible Taz KD mouse model

Utilizing the inherent genetic malleability of the inducible Taz KD mouse model, we examined the effect of removal of doxycycline from the diet following treatment to determine if the distinctive bioenergetic and lipidomic phenotype observed in the Taz KD model was restored to wild-type levels after removal of doxycycline. Following removal of the doxycycline from the diet for 2 months, analysis of glutamate stimulated adenine nucleotide translocase activity in Taz KD cardiac mitochondria, which were 6-fold increased during knockdown (Fig. 5B), were attenuated to wild-type level (supplementary Fig. IA). Additionally, high-resolution respirometry analysis of state 3 respiration under various substrates revealed an attenuation of palmitoylcarnitine, glutamate, and pyruvate/glutamate-stimulated state 3 respiration in Taz KD mice compared with wild-type mice which were removed from doxycycline treatment for 2 months (supplementary Fig. IB).

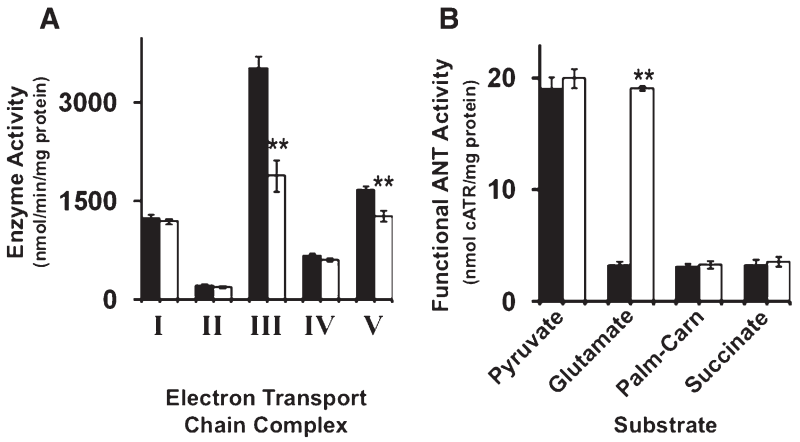

Fig. 5. Regulation of electron transport chain and adenine nucleotide translocase activities in Taz KD mice. A: Electron transport chain activities in isolated cardiac mitochondria revealed a selective decrease in Complex III and Complex V activities in the Taz KD mouse model compared with wild-type littermates. B: Analysis of the functional ANT activities driven by various substrates revealed a dramatic increase in glutamate stimulated ANT activity in the Taz KD mouse model compared with wild-type littermates. Values represent the mean enzyme activity (nmol/min/mg mitochondrial protein, ETC) or (nmol cATR/mg protein, ANT) ± S.E. (N = 5 isolated cardiac mitochondria per group; black bars, wild-type littermates; white bars, Taz KD mice). $^{**}P < 0.01$ level.

The corresponding analysis of the cardiac lipidome also demonstrated a return toward wild-type levels after removal of doxycycline from the diet. More specifically, high-resolution MDMS-SL analysis of cardiolipin revealed that after 2 months of removal of doxycycline, cardiolipin, monolysocardiolipin, and dilysocardiolipin levels returned to wild-type levels in the inducible Taz KD mouse model (supplementary Fig. IC).

TABLE 1. GSEA for myocardial transcriptome changes in the inducible Taz KD model of Barth syndrome

Gene Set Name (Number of Genes in Pathway)	Number of Genes Overlapped	*P*
Increased gene expression		
Cytosolic tRNA aminoacylation [Reactome] (23)	11	$5.15\ e^{-11}$
tRNA aminoacylation [Reactome] (40)	11	$5.28\ e^{-8}$
Aminoacyl tRNA biosynthesis [KEGG] (41)	11	$7\ e^{-8}$
Translation [Reactome] (120)	12	$7.24\ e^{-4}$
Peptide chain elongation [Reactome] (84)	9	$2.06\ e^{-3}$
Metabolism of nucleotides [Reactome] (71)	8	$2.63\ e^{-3}$
Purine metabolism [Reactome] (30)	5	$3.07\ e^{-3}$
Gene expression [Reactome] (425)	25	$4.78\ e^{-3}$
Valine, leucine, and isoleucine biosynthesis [KEGG] (11)	3	$5.21\ e^{-3}$
Amino acid synthesis and interconversion [Reactome] (12)	3	$6.77\ e^{-3}$
P53 hypoxia pathway [BioCarta] (23)	4	$6.89\ e^{-3}$
Viral mRNA translation [Reactome] (84)	8	$7.39\ e^{-3}$
GTP hydrolysis and Joining of the 60S Ribosomal Subunit	9	$9.65\ e^{-3}$
Ribosome [KEGG] (88)	8	$9.71\ e^{-3}$
Metabolism of proteins [Reactome] (215)	14	$1.44\ e^{-2}$
Formation of a pool of free 4E 40S subunits [Reactome] (95)	8	$1.5\ e^{-2}$
P53 pathway [BioCarta] (16)	3	$1.56\ e^{-2}$
ONE carbon pool of folate [KEGG] (17)	3	$1.85\ e^{-2}$
Unfolded protein response [Reactome] (19)	3	$2.5\ e^{-2}$
ATM pathway [BioCarta] (20)	3	$2.87\ e^{-2}$
EIF4 pathway [BioCarta] (24)	3	$4.62\ e^{-2}$
Decreased gene expression		
Branched chain amino acid catabolism [Reactome] (17)	3	$1.17\ e^{-2}$
IL12 pathway [BioCarta] (23)	3	$2.69\ e^{-2}$
Biopeptides pathway [BioCarta] (43)	4	$3.38\ e^{-2}$
Valine, leucine, isoleucine degradation [KEGG] (44)	4	$3.64\ e^{-2}$
CREB pathway [BioCarta] (27)	3	$4.09\ e^{-2}$

Data analyzed from GSE33452 using GSEA.

Expression of cardiolipin synthase and inhibition of iPLA$_2\gamma$ in conjunction with Tafazzin deficiency leads to altered cardiolipin and lysocardiolipin molecular species

Regulation of cardiolipin remodeling involves several enzymatic steps that could be modulated by pharmacologic intervention to decrease maladaptive cardiolipin remodeling as observed in Barth syndrome due to Tafazzin deficiency. To determine the potential therapeutic efficacy of increasing cardiolipin synthase (CLS) expression or blocking iPLA$_2\gamma$ expression as a possible treatment for Barth syndrome, we generated a doubly transgenic mouse strain crossing the inducible Taz KD mice with a transgenic mouse strain that expresses human CLS in a cardiac myocyte-specific manner which was previously demonstrated to increase cardiolipin remodeling (40). Additionally, we crossed the inducible Taz KD mice with a strain that was null for iPLA$_2\gamma$, which is involved in the generation of monolysocardiolipin for the transacylation of acyl chains for cardiolipin remodeling (56). These genetic models were used to interpret the potential to restore alterations in mitochondrial cardiolipin and lysocardiolipin composition and function due to tafazzin downregulation in the murine model of Barth syndrome. Mass spectrometric analysis of the phospholipids of wild-type, Taz KD, Taz KD crossed with CLS-TG, and Taz KD crossed with iPLA$_2\gamma$ KO male mice at 4 months of age (2 months of doxycycline treatment) revealed distinct alterations in cardiolipin and lysocardiolipin molecular species. Analysis of immature cardiolipin molecular species enriched in 16:0, 16:1, and 18:1 acyl chains revealed that increased expression of cardiolipin synthase or ablation of iPLA$_2\gamma$ under conditions of Taz KD increased the content of immature cardiolipin molecular species demonstrating that CLS and iPLA$_2\gamma$ maintain critical roles in the initial stages of cardiolipin remodeling and synthesis that is partially independent of the presence of tafazzin (**Fig. 6A**). Additionally, tetra-18:2 cardiolipin was decreased in both double cross strains compared with Taz KD alone. Analysis of other 18:2-enriched CL species such as 18:3-18:2-18:2-18:2, 18:2-18:2-18:2-18:1, and 18:2-18:2-18:1-18:1 that can serve as reservoirs for sequential remodeling to mature tetra-18:2 cardiolipin revealed selective decreases in iPLA$_2\gamma$ KO×Taz KD compared with Taz KD

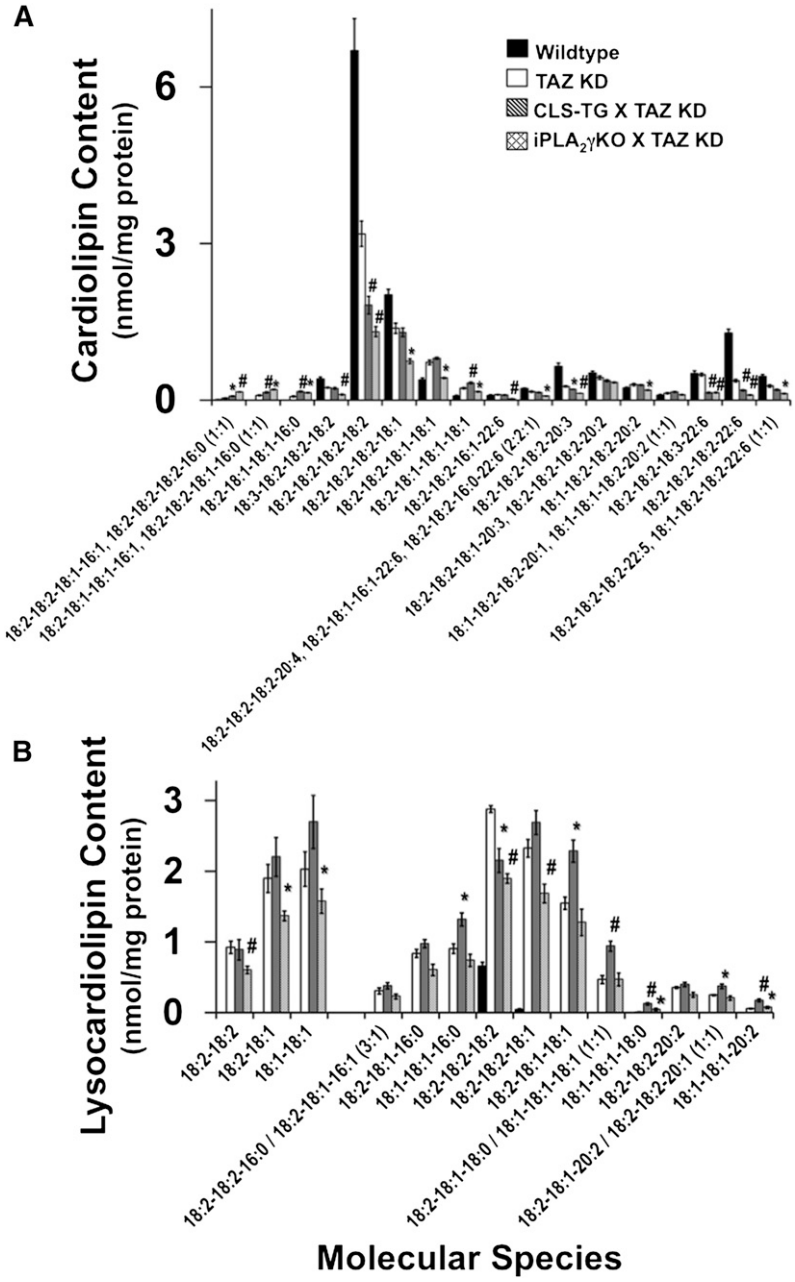

Fig. 6. Genetic manipulation of enzymes involved in cardiolipin remodeling does not prevent maladaptive remodeling of tetra-acyl cardiolipin, but instead alters lysocardiolipin molecular species. A: Quantitative analysis of cardiac cardiolipin molecular species in 4-month-old mice induced with doxycycline for 2 months (starting at 2 months of age) revealed differential alterations in molecular species in the Taz KD mice crossed with the cardiac-specific CLS-TG mice or the iPLA$_2$γ KO mouse model. B: Analysis of dilyso- and monolysocardiolipin molecular species revealed substrate specificity associated with the role of iPLA$_2$γ in cardiolipin remodeling in the absence of tafazzin as demonstrated by the iPLA$_2$γ KO×Taz KD mouse model, with fewer changes represented in the CLS-TG×Taz KD mouse model. Values represent the mean quantitative value of molecular species ± S.E. (N = 3 hearts per group; black bars, wild-type littermates; white bars, Taz KD mice; gray bars, CLS-TG×Taz KD; hatched bars, iPLA$_2$γ KO×Taz KD). $^*P < 0.05$ level, $^\#P < 0.01$ level.

alone, suggesting that iPLA$_2$γ is selectively involved in sculpting 18:2 containing immature cardiolipin species in synchrony with tafazzin to generate more mature cardiolipin molecular species by deacylation/reacylation cycling. Furthermore, cardiolipin molecular species containing 20:3 and 22:6 (such as 18:2-18:2-18:2-20:3, 18:2-18:2-18:3-22:6, and 18:2-18:2-18:2-22:6) were significantly decreased in both double cross strains compared with Taz KD alone suggesting the importance of mutual function of CLS or iPLA$_2$γ with tafazzin in cardiolipin remodeling through regulating synthesis and hydrolysis of immature cardiolipin species prepared for remodeling acylation.

MDMS-SL analysis of DLCL and MLCL revealed alterations in the selectivity of molecular species generated by the two double crosses. DLCL analysis of iPLA$_2$γ KO×Taz KD mice revealed a 30% decrease in 18:2-18:2, 18:2-18:1, and 18:1-18:1 DLCL compared with Taz KD alone, suggesting that iPLA$_2$γ plays a critical role in the initial and rapid production of DLCL for cardiolipin remodeling in an acyl chain-specific manner (Fig. 6B). DLCL molecular species in CLS-TG×Taz KD mice were similar compared with Taz KD mice. Analysis of MLCL in CLS-TG×Taz KD mice compared with Taz KD mice demonstrated an increase in immature MLCL molecular species, such as 18:1-18:1-16:0, 18:2-18:1-18:1, 18:2-18:1-18:0/18:1-18:1-18:1, and 18:1-18:1-18:0 MLCL which reflects the enhanced biosynthesis of nascent cardiolipin species resulting from the overexpression of CLS in the presence of normal phospholipase activity and deficient tafazzin activity. Alterations in DLCL in the iPLA$_2$γ KO×Taz KD mice were reflected in changes in the distribution of MLCL due to substrate selectivity as manifest by a specific decrease in 18:2-18:2-18:2 and

18:2-18:2-18:1 MLCL molecular species compared with Taz KD mice, thus demonstrating a critical role of $iPLA_2\gamma$ in the temporal and sequential remodeling of DLCL and MLCL toward a mature cardiolipin molecular species distribution.

DISCUSSION

Deconvolution of the biophysical, temporal, and integrated roles of cardiolipin, its metabolic intermediates (MLCL and DLCL), as well as the integrated processes by which cardiolipin is remodeled represents a paramount goal to understanding the mechanisms by which the mitochondrial membrane regulates bioenergetic homeostasis (57). Alterations in cardiolipin molecular speciation are evident in a variety of metabolically complex diseases such as diabetes, heart failure, Tangiers disease, cancer, hyperthyroidism, and neurodegeneration, as well as Barth syndrome (21, 33, 58–66). Thus, associating the specific roles of cardiolipin molecular species with their causative effects on bioenergetic capacity and metabolic flux is a critical objective to develop therapeutic strategies targeting the mitochondrial lipidome to reestablish bioenergetic homeostasis in a variety of complex metabolic diseases. The results of the present study investigating cardiac bioenergetic, lipidomic, and signaling mechanisms in the Taz KD mouse model of Barth syndrome demonstrate: *i*) clear resemblance of the mouse model to the human condition resulting in the accumulation of MLCL with the unexpected accumulation of DLCL; *ii*) altered distribution of acyl chains in choline and ethanolamine glycerophospholipids; *iii*) dysregulated generation of potent oxidized lipid metabolites critical for hemodynamic function; *iv*) a shift in preference for glutamate-stimulated oxidation; and *v*) an inability of the regulation of cardiolipin synthetic or mitochondrial phospholipase activities to attenuate altered cardiolipin remodeling in the tafazzin shRNA Barth syndrome mouse model.

The phenotype associated with Barth syndrome is intricately intertwined with the loss of tafazzin function, which sculpts and maintains the optimal cardiolipin molecular species distributions to coordinate metabolic homeostasis (3). The primary cause of death in those afflicted with Barth syndrome is heart failure; however, tools to experimentally dissect the complex molecular pathophysiology of this phenotype did not exist until the generation of the experimental mouse model of Barth syndrome which mimics the pathophysiologic condition in humans (23, 24). Importantly, the inducible Taz KD mouse model presents with cardiomyopathy as well as several other traits characteristic of Barth syndrome (25). A hallmark of Barth syndrome is the characteristic accumulation of MLCL, which is primarily quantified to confirm a diagnosis (67). Untargeted MDMS-SL analyses of cardiolipin species in myocardium from the Taz KD mouse model revealed a dramatic depletion of tetra-acyl CL species as well as a significant increase in MLCL species in addition to an unexpected increase in DLCL molecular species. These results provide further mechanistic insight into the role of tafazzin in the temporal lifecycle of cardiolipin as well as identify potential phospholipid substrate donors used for the transacylation of lysocardiolipin acceptors. Tafazzin deficiency results in the dynamic redistribution of unsaturated acyl chains in the mitochondrial lipidome (primarily in choline and ethanolamine glycerophospholipids) thereby impacting membrane biophysical properties and signaling through alterations as a reservoir of linoleic, arachidonic, and docosahexaenoic fatty acids for release by phospholipases and subsequent oxidation.

Interestingly, loss of tafazzin function in myocardium leads to changes in the mitochondrial lipidome resulting in the dysregulated generation of potent oxidized derivatives of polyunsaturated fatty acids. Thus, tafazzin serves as a previously unrecognized regulator of multiple processes leading to changes in the vasoresponsive and inflammatory capacity of myocardium in Barth syndrome presumably through its ability to influence acyl chain location in phospholipids, the activity of distinct phospholipases, and/or channeling of polyunsaturated fatty acid substrates to a variety of lipoxygenases, cyclooxygenases, and cytochrome P450 enzymes. We specifically note that oxidized lipid metabolites also serve as key regulators of ion channel function as well as calcium homeostasis which likely modulate myocardial function in complex metabolic disease such as Barth syndrome (50, 51, 68). Additionally, because these oxidized molecules originate from the mitochondria, it would appear that mitochondria in Barth syndrome may also impact mitokine signaling precipitating maladaptive alterations in lipid metabolism, signaling, and bioenergetics.

A comprehensive interrogation of mitochondrial bioenergetics in Barth syndrome myocardium has previously been hindered due to lack of sufficient appropriate specimens to adequately investigate the full spectrum of bioenergetic capacity. The inducible Taz KD mouse model described in the present study represents a valuable tool for investigation of mitochondrial function as an experimental model of Barth syndrome. Herein, we demonstrate that cardiac mitochondria isolated from tafazzin-deficient mice are capable of undergoing effective coupled respiration even with a severe deficiency of mature tetra-acyl cardiolipin as well as the accompanied accumulation of lysocardiolipin species (MLCL and DLCL). High-resolution respirometric analysis of isolated cardiac mitochondria revealed deficiencies in fatty acid oxidation, which was compensated by increased glutamate-stimulated metabolism, thus demonstrating a characteristic shift in the flux of the TCA cycle and substrate preference of cardiac mitochondria to select amino acid fermentation over the normally preferred fatty acid metabolism. This phenomenon was further supported by alterations in key transcriptional pathways indicating that tafazzin deficiency precipitates altered cardiolipin remodeling thereby resulting in a preferential substrate shift toward de novo amino acid biosynthesis as well as increased amino acid utilization by the TCA cycle. These data appear to support the previous finding of increased whole-body protein

catabolism in Barth syndrome patients (69). Pyruvate metabolism was unchanged in tafazzin-deficient mouse mitochondria indicating that cardiolipin is not obligatory for pyruvate utilization, but does appear essential for fatty acid oxidation. This is predominantly due to the unique role of cardiolipin in maintaining the mitochondrial trifunctional complex, which is essential for efficient fatty acid oxidation (70) and cannot be compensated with lysocardiolipin species (i.e., MLCL and DLCL).

Alterations in cardiolipin have previously been associated with the regulation of electron transport chain complex components as well as several other pivotal metabolic enzymes in the mitochondrial membrane (71–77). Previously, a decrease in Complex III activity in Barth syndrome fibroblasts from two patients was reported in addition to several other minor metabolic deficiencies (78). In addition, whole-body and oxidative capacity, indirect measurements of mitochondrial function, were significantly decreased during exercise in humans with Barth syndrome (5). However, mitochondrial function in highly metabolically active tissues such as myocardium is closely integrated with physiologic demands and likely determines the underlying alterations in bioenergetic capacity in vivo in Barth syndrome patients. To identify the upstream mechanism underlying the shift in preference toward glutamate oxidation in the Taz KD mouse, we investigated the adenine nucleotide translocase which exhibits differences in substrate selectivity between various tissues as well as a dependence on cardiolipin for its catalytic activity (53, 74, 79, 80). The reorganization of cardiolipin and lysocardiolipin molecular species in this Barth syndrome mouse model likely precipitates a dramatic shift in glutamate preference driving ADP/ATP exchange in the mitochondria, thus linking cardiolipin to the substrate-specific regulation of respiration.

A distinct advantage of utilizing an inducible shRNA knockdown mouse model of Barth syndrome is its ability to be combined with other genetic tools to investigate therapeutic strategies to target cardiolipin metabolism or other aspects of the disease. Recently, genetic models either expressing human CLS in myocardium or eliminating iPLA$_2\gamma$ expression have been investigated regarding their participation in cardiolipin biosynthesis and remodeling in the heart (40, 56). Characterization of the cardiac-specific human CLS-transgenic mouse revealed a significant increase in CL remodeling and tetra-18:2 cardiolipin content compared with wild-type mice, thus identifying a compensatory mechanism to ameliorate the deficiency in tetra-18:2 cardiolipin found in Barth syndrome (40). Furthermore, phospholipases have been suggested as pharmacologic targets to prevent deacylation of cardiolipin, thereby preventing monolysocardiolipin accumulation which is a hallmark characteristic of Barth syndrome (81–83). In the current study, transgenic expression of human CLS in myocardium or ablation of iPLA$_2\gamma$ in conjunction with tafazzin deficiency did not prevent the decreased cardiolipin content (predominantly tetra-18:2 CL) present in the Taz KD mouse, thus demonstrating that CLS and/or iPLA$_2\gamma$ are likely independent of tafazzin as components of the initial remodeling machinery to maintain a homeostatic balance of cardiolipin molecular species.

Although the doxycycline-inducible knockdown construct provides a malleable genetic tool for the investigation of bioenergetic and lipidomic remodeling associated with tafazzin deficiency, several additional caveats should be considered in regard to the use of tetracycline-inducible promoters used in numerous genetic models. Tetracyclines, including doxycycline, have previously been associated with modulation of secretory phospholipases (84, 85) as well as the inhibition of metalloproteinases, downregulation of cytokines, and cell proliferation (86), all of which should be considered in regard to the phenotypic characterization of the Barth syndrome mouse model. Because the inducible Taz KD mice were compared with wild-type age-matched littermates also fed a doxycycline-enriched diet, the differential phenotype displayed represents the pathological changes induced by cardiac myocyte tafazzin deficiency. Furthermore, it was previously reported that the level at which doxycycline or tetracyclines inhibited these biological processes in vitro far exceeds the pharmacological dose that would be administered in vivo (86, 87), thus demonstrating the strength of the pathological findings manifest during tafazzin deficiency that are reversible upon its reexpression.

In summary, the inducible Taz KD mouse represents an efficacious model system that recapitulates many of the underlying myocardial lipidomic and bioenergetic phenotypes present in Barth syndrome. Moreover, the use of this model in conjunction with integrated analytic technologies has allowed increased understanding of the complexity of molecular alterations resulting from tafazzin loss of function that likely exist in Barth syndrome patients. Our results demonstrate that tafazzin loss of function results in profound alterations in the myocardial lipidome, deleterious changes in bioenergetic flux, and altered signaling processes that collectively contribute to the pathology of Barth syndrome.

REFERENCES

1. Christodoulou, J., R. R. McInnes, V. Jay, G. Wilson, L. E. Becker, D. C. Lehotay, B. A. Platt, P. J. Bridge, B. H. Robinson, and J. T. Clarke. 1994. Barth syndrome: clinical observations and genetic linkage studies. *Am. J. Med. Genet.* **50:** 255–264.
2. Bione, S., P. D'Adamo, E. Maestrini, A. K. Gedeon, P. A. Bolhuis, and D. Toniolo. 1996. A novel X-linked gene, G4.5, is responsible for Barth syndrome. *Nat. Genet.* **12:** 385–389.
3. Xu, Y., A. Malhotra, M. Ren, and M. Schlame. 2006. The enzymatic function of tafazzin. *J. Biol. Chem.* **281:** 39217–39224.
4. Gonzalez, I. L. 2005. Barth syndrome: TAZ gene mutations, mRNAs, and evolution. *Am. J. Med. Genet.* **134:** 409–414.
5. Spencer, C. T., B. J. Byrne, R. M. Bryant, R. Margossian, M. Maisenbacher, P. Breitenger, P. B. Benni, S. Redfearn, E. Marcus, and W. T. Cade. 2011. Impaired cardiac reserve and severely diminished skeletal muscle O(2) utilization mediate exercise intolerance in Barth syndrome. *Am. J. Physiol. Heart Circ. Physiol.* **301:** H2122–H2129.
6. Hauff, K. D., and G. M. Hatch. 2006. Cardiolipin metabolism and Barth syndrome. *Prog. Lipid Res.* **45:** 91–101.
7. Schlame, M., and M. Ren. 2006. Barth syndrome, a human disorder of cardiolipin metabolism. *FEBS Lett.* **580:** 5450–5455.
8. Xu, Y., R. I. Kelley, T. J. Blanck, and M. Schlame. 2003. Remodeling of cardiolipin by phospholipid transacylation. *J. Biol. Chem.* **278:** 51380–51385.

9. Houtkooper, R. H., M. Turkenburg, B. T. Poll-The, D. Karall, C. Perez-Cerda, A. Morrone, S. Malvagia, R. J. Wanders, W. Kulik, and F. M. Vaz. 2009. The enigmatic role of tafazzin in cardiolipin metabolism. *Biochim. Biophys. Acta.* **1788:** 2003–2014.
10. Furt, F., and P. Moreau. 2009. Importance of lipid metabolism for intracellular and mitochondrial membrane fusion/fission processes. *Int. J. Biochem. Cell Biol.* **41:** 1828–1836.
11. Daum, G. 1985. Lipids of mitochondria. *Biochim. Biophys. Acta.* **822:** 1–42.
12. Hoch, F. L. 1992. Cardiolipins and biomembrane function. *Biochim. Biophys. Acta.* **1113:** 71–133.
13. Huang, H., and M. A. Frohman. 2009. Lipid signaling on the mitochondrial surface. *Biochim. Biophys. Acta.* **1791:** 839–844.
14. Herzig, S., and J. C. Martinou. 2008. Mitochondrial dynamics: to be in good shape to survive. *Curr. Mol. Med.* **8:** 131–137.
15. Dahlberg, M. 2007. Polymorphic phase behavior of cardiolipin derivatives studied by coarse-grained molecular dynamics. *J. Phys. Chem. B.* **111:** 7194–7200.
16. Claypool, S. M., and C. M. Koehler. 2012. The complexity of cardiolipin in health and disease. *Trends Biochem. Sci.* **37:** 32–41.
17. Pangborn, M. 1942. Isolation and purification of a serologically active phospholipid from beef heart. *J. Biol. Chem.* **143:** 247–256.
18. Schlame, M., and M. Ren. 2009. The role of cardiolipin in the structural organization of mitochondrial membranes. *Biochim. Biophys. Acta.* **1788:** 2080–2083.
19. Schlame, M., M. Ren, Y. Xu, M. L. Greenberg, and I. Haller. 2005. Molecular symmetry in mitochondrial cardiolipins. *Chem. Phys. Lipids.* **138:** 38–49.
20. Gebert, N., A. S. Joshi, S. Kutik, T. Becker, M. McKenzie, X. Li Guan, V. P. Mooga, D. A. Stroud, G. Kulkarni, M. R. Wenk, et al. 2009. Mitochondrial cardiolipin involved in outer-membrane protein biogenesis: implications for Barth syndrome. *Curr. Biol.* **19:** 2133–2139.
21. Chicco, A. J., and G. C. Sparagna. 2007. Role of cardiolipin alterations in mitochondrial dysfunction and disease. *Am. J. Physiol. Cell Physiol.* **292:** C33–C44.
22. Hatch, G. M. 1998. Cardiolipin: biosynthesis, remodeling and trafficking in the heart and mammalian cells (Review). *Int. J. Mol. Med.* **1:** 33–41.
23. Soustek, M. S., D. J. Falk, C. S. Mah, M. J. Toth, M. Schlame, A. S. Lewin, and B. J. Byrne. 2011. Characterization of a transgenic short hairpin RNA-induced murine model of tafazzin deficiency. *Hum. Gene Ther.* **22:** 865–871.
24. Acehan, D., F. Vaz, R. H. Houtkooper, J. James, V. Moore, C. Tokunaga, W. Kulik, J. Wansapura, M. J. Toth, A. Strauss, et al. 2011. Cardiac and skeletal muscle defects in a mouse model of human Barth syndrome. *J. Biol. Chem.* **286:** 899–908.
25. Phoon, C. K., D. Acehan, M. Schlame, D. L. Stokes, I. Edelman-Novemsky, D. Yu, Y. Xu, N. Viswanathan, and M. Ren. 2012. Tafazzin knockdown in mice leads to a developmental cardiomyopathy with early diastolic dysfunction preceding myocardial noncompaction. *J. Am. Heart Assoc.* **1:** jah3-000455.
26. Kiebish, M. A., R. Bell, K. Yang, T. Phan, Z. Zhao, W. Ames, T. N. Seyfried, R. W. Gross, J. H. Chuang, and X. Han. 2010. Dynamic simulation of cardiolipin remodeling: greasing the wheels for an interpretative approach to lipidomics. *J. Lipid Res.* **51:** 2153–2170.
27. Mancuso, D. J., H. F. Sims, K. Yang, M. A. Kiebish, X. Su, C. M. Jenkins, S. Guan, S. H. Moon, T. Pietka, F. Nassir, et al. 2010. Genetic ablation of calcium-independent phospholipase A2gamma prevents obesity and insulin resistance during high fat feeding by mitochondrial uncoupling and increased adipocyte fatty acid oxidation. *J. Biol. Chem.* **285:** 36495–36510.
28. Yang, K., H. Cheng, R. W. Gross, and X. Han. 2009. Automated lipid identification and quantification by multidimensional mass spectrometry-based shotgun lipidomics. *Anal. Chem.* **81:** 4356–4368.
29. Han, X., K. Yang, J. Yang, H. Cheng, and R. W. Gross. 2006. Shotgun lipidomics of cardiolipin molecular species in lipid extracts of biological samples. *J. Lipid Res.* **47:** 864–879.
30. Bollinger, J. G., W. Thompson, Y. Lai, R. C. Oslund, T. S. Hallstrand, M. Sadilek, F. Turecek, and M. H. Gelb. 2010. Improved sensitivity mass spectrometric detection of eicosanoids by charge reversal derivatization. *Anal. Chem.* **82:** 6790–6796.
31. Jüllig, M., A. J. Hickey, C. C. Chai, G. L. Skea, M. J. Middleditch, S. Costa, S. Y. Choong, A. R. Philips, and G. J. Cooper. 2008. Is the failing heart out of fuel or a worn engine running rich? A study of mitochondria in old spontaneously hypertensive rats. *Proteomics.* **8:** 2556–2572.
32. Birch-Machin, M. A., and D. M. Turnbull. 2001. Assaying mitochondrial respiratory complex activity in mitochondria isolated from human cells and tissues. *Methods Cell Biol.* **65:** 97–117.
33. Ellis, C. E., E. J. Murphy, D. C. Mitchell, M. Y. Golovko, F. Scaglia, G. C. Barcelo-Coblijn, and R. L. Nussbaum. 2005. Mitochondrial lipid abnormality and electron transport chain impairment in mice lacking alpha-synuclein. *Mol. Cell. Biol.* **25:** 10190–10201.
34. King, T. E. 1967. Preparation of succinate dehydrogenase and reconstitution of succinate oxidase. *In* Methods in Enzymology: Oxidation and Phosphorylation. R. Estabrook and M. Pullman, editors. Academic Press, New York. 322–331.
35. Degli Esposti, M. 2001. Assessing functional integrity of mitochondria in vitro and in vivo. *Methods Cell Biol.* **65:** 75–96.
36. Yonetan, T. 1967. Cytochrome oxidase: beef heart. *In* Methods in Enzymology: Oxidation and Phosphorylation. R. Estabrook and M. Pullman, editors. Academic Press, New York. 332–335.
37. Bosetti, F., G. Yu, R. Zucchi, S. Ronca-Testoni, and G. Solaini. 2000. Myocardial ischemic preconditioning and mitochondrial F1F0-ATPase activity. *Mol. Cell. Biochem.* **215:** 31–37.
38. Kipp, J. L., and V. D. Ramirez. 2001. Effect of estradiol, diethylstilbestrol, and resveratrol on F0F1-ATPase activity from mitochondrial preparations of rat heart, liver, and brain. *Endocrine.* **15:** 165–175.
39. Zheng, J., and V. D. Ramirez. 1999. Rapid inhibition of rat brain mitochondrial proton F0F1-ATPase activity by estrogens: comparison with Na+, K+ -ATPase of porcine cortex. *Eur. J. Pharmacol.* **368:** 95–102.
40. Kiebish, M. A., K. Yang, H. F. Sims, C. M. Jenkins, X. Liu, D. J. Mancuso, Z. Zhao, S. Guan, D. R. Abendschein, X. Han, et al. 2012. Myocardial regulation of lipidomic flux by cardiolipin synthase: setting the beat for bioenergetic efficiency. *J. Biol. Chem.* **287:** 25086–25097.
41. Roussel, D., F. Chainier, J. Rouanet, and H. Barre. 2000. Increase in the adenine nucleotide translocase content of duckling subsarcolemmal mitochondria during cold acclimation. *FEBS Lett.* **477:** 141–144.
42. Oliveira, P. J., and K. B. Wallace. 2006. Depletion of adenine nucleotide translocator protein in heart mitochondria from doxorubicin-treated rats–relevance for mitochondrial dysfunction. *Toxicology.* **220:** 160–168.
43. Gellerich, F. N., W. S. Kunz, and R. Bohnensack. 1990. Estimation of flux control coefficients from inhibitor titrations by non-linear regression. *FEBS Lett.* **274:** 167–170.
44. Guillet, V., N. Gueguen, C. Verny, M. Ferre, C. Homedan, D. Loiseau, V. Procaccio, P. Amati-Bonneau, D. Bonneau, P. Reynier, et al. 2010. Adenine nucleotide translocase is involved in a mitochondrial coupling defect in MFN2-related Charcot-Marie-Tooth type 2A disease. *Neurogenetics.* **11:** 127–133.
45. Brown, J. C., A. R. Gerson, and J. F. Staples. 2007. Mitochondrial metabolism during daily torpor in the dwarf Siberian hamster: role of active regulated changes and passive thermal effects. *Am. J. Physiol. Regul. Integr. Comp. Physiol.* **293:** R1833–R1845.
46. Valianpour, F., R. J. Wanders, H. Overmars, P. Vreken, A. H. Van Gennip, F. Baas, B. Plecko, R. Santer, K. Becker, and P. G. Barth. 2002. Cardiolipin deficiency in X-linked cardioskeletal myopathy and neutropenia (Barth syndrome, MIM 302060): a study in cultured skin fibroblasts. *J. Pediatr.* **141:** 729–733.
47. Wang, R., J. T. Kern, T. L. Goodfriend, D. L. Ball, and H. Luesch. 2009. Activation of the antioxidant response element by specific oxidized metabolites of linoleic acid. *Prostaglandins Leukot. Essent. Fatty Acids.* **81:** 53–59.
48. Searles, C. D. 2006. Transcriptional and posttranscriptional regulation of endothelial nitric oxide synthase expression. *Am. J. Physiol. Cell Physiol.* **291:** C803–C816.
49. Obinata, H., and T. Izumi. 2009. G2A as a receptor for oxidized free fatty acids. *Prostaglandins Other Lipid Mediat.* **89:** 66–72.
50. Li, N., J. Y. Liu, H. Qiu, T. R. Harris, P. Sirish, B. D. Hammock, and N. Chiamvimonvat. 2011. Use of metabolomic profiling in the study of arachidonic acid metabolism in cardiovascular disease. *Congest. Heart Fail.* **17:** 42–46.
51. Sudhahar, V., S. Shaw, and J. D. Imig. 2010. Epoxyeicosatrienoic acid analogs and vascular function. *Curr. Med. Chem.* **17:** 1181–1190.
52. Brustovetsky, N., and M. Klingenberg. 1996. Mitochondrial ADP/ATP carrier can be reversibly converted into a large channel by Ca2+. *Biochemistry.* **35:** 8483–8488.
53. Claypool, S. M., Y. Oktay, P. Boontheung, J. A. Loo, and C. M. Koehler. 2008. Cardiolipin defines the interactome of the major

ADP/ATP carrier protein of the mitochondrial inner membrane. *J. Cell Biol.* **182:** 937–950.
54. Subramanian, A., P. Tamayo, V. K. Mootha, S. Mukherjee, B. L. Ebert, M. A. Gillette, A. Paulovich, S. L. Pomeroy, T. R. Golub, E. S. Lander, et al. 2005. Gene set enrichment analysis: a knowledge-based approach for interpreting genome-wide expression profiles. *Proc. Natl. Acad. Sci. USA.* **102:** 15545–15550.
55. Mootha, V. K., C. M. Lindgren, K. F. Eriksson, A. Subramanian, S. Sihag, J. Lehar, P. Puigserver, E. Carlsson, M. Ridderstrale, E. Laurila, et al. 2003. PGC-1alpha-responsive genes involved in oxidative phosphorylation are coordinately downregulated in human diabetes. *Nat. Genet.* **34:** 267–273.
56. Mancuso, D. J., H. F. Sims, X. Han, C. M. Jenkins, S. P. Guan, K. Yang, S. H. Moon, T. Pietka, N. A. Abumrad, P. H. Schlesinger, et al. 2007. Genetic ablation of calcium-independent phospholipase A2gamma leads to alterations in mitochondrial lipid metabolism and function resulting in a deficient mitochondrial bioenergetic phenotype. *J. Biol. Chem.* **282:** 34611–34622.
57. Osman, C., D. R. Voelker, and T. Langer. 2011. Making heads or tails of phospholipids in mitochondria. *J. Cell Biol.* **192:** 7–16.
58. Fobker, M., R. Voss, H. Reinecke, C. Crone, G. Assmann, and M. Walter. 2001. Accumulation of cardiolipin and lysocardiolipin in fibroblasts from Tangier disease subjects. *FEBS Lett.* **500:** 157–162.
59. Han, X., J. Yang, H. Cheng, K. Yang, D. R. Abendschein, and R. W. Gross. 2005. Shotgun lipidomics identifies cardiolipin depletion in diabetic myocardium linking altered substrate utilization with mitochondrial dysfunction. *Biochemistry.* **44:** 16684–16694.
60. Joshi, D. C., and J. C. Bakowska. 2011. SPG20 protein spartin associates with cardiolipin via its plant-related senescence domain and regulates mitochondrial Ca2+ homeostasis. *PLoS ONE.* **6:** e19290.
61. Pope, S., J. M. Land, and S. J. Heales. 2008. Oxidative stress and mitochondrial dysfunction in neurodegeneration; cardiolipin a critical target? *Biochim. Biophys. Acta.* **1777:** 794–799.
62. Sparagna, G. C., A. J. Chicco, R. C. Murphy, M. R. Bristow, C. A. Johnson, M. L. Rees, M. L. Maxey, S. A. McCune, and R. L. Moore. 2007. Loss of cardiac tetralinoleoyl cardiolipin in human and experimental heart failure. *J. Lipid Res.* **48:** 1559–1570.
63. Kiebish, M. A., X. Han, H. Cheng, J. H. Chuang, and T. N. Seyfried. 2008. Cardiolipin and electron transport chain abnormalities in mouse brain tumor mitochondria: lipidomic evidence supporting the Warburg theory of cancer. *J. Lipid Res.* **49:** 2545–2556.
64. Mutter, T., V. W. Dolinsky, B. J. Ma, W. A. Taylor, and G. M. Hatch. 2000. Thyroxine regulation of monolysocardiolipin acyltransferase activity in rat heart. *Biochem. J.* **346:** 403–406.
65. Vreken, P., F. Valianpour, L. G. Nijtmans, L. A. Grivell, B. Plecko, R. J. Wanders, and P. G. Barth. 2000. Defective remodeling of cardiolipin and phosphatidylglycerol in Barth syndrome. *Biochem. Biophys. Res. Commun.* **279:** 378–382.
66. Schlame, M., J. A. Towbin, P. M. Heerdt, R. Jehle, S. DiMauro, and T. J. Blanck. 2002. Deficiency of tetralinoleoyl-cardiolipin in Barth syndrome. *Ann. Neurol.* **51:** 634–637.
67. Houtkooper, R. H., R. J. Rodenburg, C. Thiels, H. van Lenthe, F. Stet, B. T. Poll-The, J. E. Stone, C. G. Steward, R. J. Wanders, J. Smeitink, et al. 2009. Cardiolipin and monolysocardiolipin analysis in fibroblasts, lymphocytes, and tissues using high-performance liquid chromatography-mass spectrometry as a diagnostic test for Barth syndrome. *Anal. Biochem.* **387:** 230–237.
68. Wang, D., V. V. Patel, E. Ricciotti, R. Zhou, M. D. Levin, E. Gao, Z. Yu, V. A. Ferrari, M. M. Lu, J. Xu, et al. 2009. Cardiomyocyte cyclooxygenase-2 influences cardiac rhythm and function. *Proc. Natl. Acad. Sci. USA.* **106:** 7548–7552.
69. Cade, W. T., C. T. Spencer, D. N. Reeds, A. D. Waggoner, R. O'Connor, M. Maisenbacher, J. R. Crowley, B. J. Byrne, and L. R. Peterson. 2013. Substrate metabolism during basal and hyperinsulinemic conditions in adolescents and young-adults with Barth syndrome. *J. Inherit. Metab. Dis.* **36:** 91–101.
70. Fould, B., V. Garlatti, E. Neumann, D. Fenel, C. Gaboriaud, and G. J. Arlaud. 2010. Structural and functional characterization of the recombinant human mitochondrial trifunctional protein. *Biochemistry.* **49:** 8608–8617.
71. Fry, M., and D. E. Green. 1980. Cardiolipin requirement by cytochrome oxidase and the catalytic role of phospholipid. *Biochem. Biophys. Res. Commun.* **93:** 1238–1246.
72. Fry, M., and D. E. Green. 1981. Cardiolipin requirement for electron transfer in complex I and III of the mitochondrial respiratory chain. *J. Biol. Chem.* **256:** 1874–1880.
73. Houtkooper, R. H., and F. M. Vaz. 2008. Cardiolipin, the heart of mitochondrial metabolism. *Cell. Mol. Life Sci.* **65:** 2493–2506.
74. Klingenberg, M. 2009. Cardiolipin and mitochondrial carriers. *Biochim. Biophys. Acta.* **1788:** 2048–2058.
75. López-Moratalla, N., J. L. Segovia, and E. Santiago. 1973. Specificity of association between linoleylcardiolipins and mitochondrial ATPase. *Rev. Esp. Fisiol.* **29:** 329–334.
76. Santiago, E., N. Lopez-Moratalla, and J. F. Segovia. 1973. Correlation between losses of mitochondrial ATPase activity and cardiolipin degradation. *Biochem. Biophys. Res. Commun.* **53:** 439–445.
77. Yang, H., Y. Huang, X. Zhang, and F. Yang. 2001. Cardiolipin is essential for higher proton translocation activity of reconstituted F(0). *Sci. China C Life Sci.* **44:** 146–155.
78. Barth, P. G., C. Van den Bogert, P. A. Bolhuis, H. R. Scholte, A. H. van Gennip, R. B. Schutgens, and A. G. Ketel. 1996. X-linked cardioskeletal myopathy and neutropenia (Barth syndrome): respiratory-chain abnormalities in cultured fibroblasts. *J. Inherit. Metab. Dis.* **19:** 157–160.
79. Bohnensack, R., F. N. Gellerich, L. Schild, and W. Kunz. 1990. The function of the adenine nucleotide translocator in the control of oxidative phosphorylation. *Biochim. Biophys. Acta.* **1018:** 182–184.
80. Beyer, K., and M. Klingenberg. 1985. ADP/ATP carrier protein from beef heart mitochondria has high amounts of tightly bound cardiolipin, as revealed by 31P nuclear magnetic resonance. *Biochemistry.* **24:** 3821–3826.
81. Malhotra, A., I. Edelman-Novemsky, Y. Xu, H. Plesken, J. Ma, M. Schlame, and M. Ren. 2009. Role of calcium-independent phospholipase A2 in the pathogenesis of Barth syndrome. *Proc. Natl. Acad. Sci. USA.* **106:** 2337–2341.
82. Seleznev, K., C. Zhao, X. H. Zhang, K. Song, and Z. A. Ma. 2006. Calcium-independent phospholipase A2 localizes in and protects mitochondria during apoptotic induction by staurosporine. *J. Biol. Chem.* **281:** 22275–22288.
83. Zachman, D. K., A. J. Chicco, S. A. McCune, R. C. Murphy, R. L. Moore, and G. C. Sparagna. 2010. The role of calcium-independent phospholipase A2 in cardiolipin remodeling in the spontaneously hypertensive heart failure rat heart. *J. Lipid Res.* **51:** 525–534.
84. Dalm, D., G. J. Palm, A. Aleksandrov, T. Simonson, and W. Hinrichs. 2010. Nonantibiotic properties of tetracyclines: structural basis for inhibition of secretory phospholipase A2. *J. Mol. Biol.* **398:** 83–96.
85. McHowat, J., L. M. Swift, K. N. Crown, and N. A. Sarvazyan. 2004. Changes in phospholipid content and myocardial calcium-independent phospholipase A2 activity during chronic anthracycline administration. *J. Pharmacol. Exp. Ther.* **311:** 736–741.
86. Korting, H. C., and C. Schöllmann. 2009. The significance of itraconazole for treatment of fungal infections of skin, nails and mucous membranes. *J. Dtsch. Dermatol. Ges.* **7:** 11–9, 11–20.
87. Mäkelä, A., T. Kuusi, and T. Schröder. 1997. Inhibition of serum phospholipase-A2 in acute pancreatitis by pharmacological agents in vitro. *Scand. J. Clin. Lab. Invest.* **57:** 401–407.